Journal of the Optical Society of America A
OPTICS, IMAGE SCIENCE, AND VISION

Efficient evaluation of Sommerfeld integrals for the optical simulation of many scattering particles in planarly layered media

AMOS EGEL,[1,2,*] SIEGFRIED W. KETTLITZ,[1] AND ULI LEMMER[1,2]

[1]Light Technology Institute, Karlsruhe Institute of Technology, 76131 Karlsruhe, Germany
[2]Institute of Microstructure Technology, Karlsruhe Institute of Technology, 76131 Karlsruhe, Germany
*Corresponding author: amos.egel@kit.edu

Received 7 January 2016; revised 10 February 2016; accepted 19 February 2016; posted 19 February 2016 (Doc. ID 256908); published 22 March 2016

A strategy for the efficient numerical evaluation of Sommerfeld integrals in the context of electromagnetic scattering at particles embedded in a plane parallel layer system is presented. The scheme relies on a lookup-table approach in combination with an asymptotic approximation of the Bessel function in order to enable the use of fast Fourier transformation. Accuracy of the algorithm is enhanced by means of singularity extraction and a novel technique to treat the integrand at small arguments. For short particle distances, this method is accomplished by a slower but more robust direct integration along a deflected contour. As an example, we investigate enhanced light extraction from an organic light-emitting diode by optical scattering particles. The calculations are discussed with respect to accuracy and computing time. By means of the present strategy, an accurate evaluation of the scattered field for several thousand wavelength scale particles can be achieved within a few hours on a conventional workstation computer.

OCIS codes: (290.5850) Scattering, particles; (290.5825) Scattering theory; (310.6845) Thin film devices and applications; (230.3670) Light-emitting diodes.

http://dx.doi.org/10.1364/JOSAA.33.000698

1. INTRODUCTION

Scattering particles embedded in thin film systems find use in various applications, e.g., for light management in optoelectronic devices such as organic light-emitting diodes (OLEDs) or thin film solar cells [1–4]. In general, the purpose is to couple electromagnetic waveguide modes to the far field. To understand the involved mechanisms and to optimize the device efficiency, optical simulations are of high value. A particularly suitable modeling approach utilizes the expansion of the scattered electric field in spherical vector wave functions relative to the particles' center positions such that the scattering at each individual particle can be treated within the T-matrix formalism [5,6]. In order to account for the propagation in the plane parallel layer system (e.g., by means of the scattering matrix formalism [7]), the fields also need to be expressed as a superposition of plane waves (alternatively, cylindrical waves can be used). Transformation formulae between plane and spherical wave functions allow an integral formalism, taking advantage of each representation [8–13].

For a large number of scattering particles, the computation of the mutual particle coupling coefficients involves a significant effort because numerical quadrature of many so-called Sommerfeld integrals is required. These 1D highly oscillatory integrals are characteristic for the propagation of spherical waves near plane interfaces [14] and have been extensively studied in literature (for an overview, see [15,16]). The majority of publications refer to the problem of vertical or horizontal dipole radiation near an interface, which leads to integrals involving Bessel functions of order zero or one, respectively. However, the description of wavelength-scale particles within the T-matrix formalism requires higher-order multipole terms such that the suggested numerical approaches need to be adapted to the case of higher-order Bessel functions [17]. In addition, the number of particle coupling coefficients scales quadratic with the number of particles. As a consequence, the number of required Sommerfeld integral evaluations can exceed several billion for the case of a few thousand scattering particles. The possibility to reuse intermediate results (e.g., integrand evaluations) is then critical for the overall computational efficiency.

The aim of this paper is to present an efficient computational strategy for the Sommerfeld integration in the given context. The approach involves the fast Fourier transform (FFT) in order to simultaneously compute multiple Sommerfeld integrals. To increase the accuracy, we employ singularity extraction techniques

that are adapted to the case of higher-order multipole interaction. The Bessel functions are approximated by an asymptotic expression that is valid in the large argument limit. A newly developed technique is therefore applied to suppress the integrand in the small argument limit. The FFT-based quadrature approach is complemented by the more robust but slower direct integration along a deflected contour in order to account for small particle distances, as here the asymptotic expansion cannot provide reliable results. By means of this dual approach, a 2D lookup table is computed, serving for interpolation of the actual particle coupling coefficients.

The paper is organized as follows: In Section 2, we give a brief overview on the theoretical framework describing the scattering problem. Section 3 introduces lookup tables for an acceleration of the coupling matrix assembly. The actual scheme for the evaluation of the Sommerfeld integrals is presented in Section 4. In Section 5, exemplary calculation results are presented and discussed with respect to numerical accuracy and computational effort, before we finally draw conclusions in Section 6.

2. MULTIPLE SCATTERING IN PLANARLY LAYERED MEDIA

The system under study is given by a distribution of N particles located inside one layer within a system of plane parallel homogeneous layers. It is illuminated by a monochromatic primary electromagnetic excitation with angular frequency ω, e.g., an incoming plane wave, a Gaussian beam or the wave emitted by a point dipole source. For a fixed particle s, the field in the scattering layer can be written as the sum of a regular part (incoming field):

$$\mathbf{E}^s_{\mathrm{reg}}(\mathbf{r}) = \sum_n a^s_n \mathbf{M}^{(1)}_n(\mathbf{r} - \mathbf{r}_s), \tag{1}$$

and an outgoing part (scattered field):

$$\mathbf{E}^s_{\mathrm{scat}}(\mathbf{r}) = \sum_n b^s_n \mathbf{M}^{(3)}_n(\mathbf{r} - \mathbf{r}_s), \tag{2}$$

where $\mathbf{M}^{(\nu)}_n(\mathbf{r} - \mathbf{r}_s)$ stands for the regular ($\nu = 1$) or outgoing ($\nu = 3$) spherical vector wave functions (SVWFs) relative to the particle's center position $\mathbf{r}_s$. The expansion coefficients a and b carry two indices, s and n. Whereas s indicates the particle to which a and b refer, $n = (p, l, m)$ is a multi-index denoting the polarization p and multipole coefficients $l = 1, \ldots$ and $m = -l, \ldots, l$. A definition of the SVWFs is given in Appendix A. The regular part includes the initial excitation and the scattered field from all other particles as well the layer system's reflections of all particles' (including s) scattered field. The computation of the electric field reduces to the problem of simultaneously calculating the incoming and scattered field coefficients a^s_n and b^s_n for all particles s, which can be achieved by solving the following self consistent linear system:

$$b^s_n = \sum_{n'} T^s_{nn'} a^s_{n'}, \tag{3}$$

$$a^s_n = \sum_{s'} \sum_{n'} W^{ss'}_{nn'} b^{s'}_{n'} + a^{s,\mathrm{in}}_n. \tag{4}$$

Equation (3) defines the transition matrix $T^s_{nn'}$ (T-matrix) of particle s. The T-matrix incorporates the scattering behavior of the individual particles and depends on their shape, size, and refractive index. For a broad class of particles (which can be dielectric or metallic), efficient and robust numerical techniques have been presented for its computation (see [6] for a collection of references). In Eq. (4), $a^{s,\mathrm{in}}_n$ denotes the spherical wave coefficients representing the initial excitation, which is known *a priori*, whereas the coupling matrix $W^{ss'}_{nn'}$ states how the field excited by an outgoing SVWF emitted from particle s' will be perceived as a linear combination of regular SVWFs at particle s. As the entries of $T^s_{nn'}$ decrease rapidly for large n and n', it is in practice sufficient to truncate the expansions Eqs. (1) and (2) at some $n_{\max}$ that depends on the wavelength and particle size and material, rendering a finite system of linear equations in Eqs. (3) and (4). Note that, when the latter is solved, multiple scattering between the particles is automatically accounted for, without the need of a scattering order approximation.

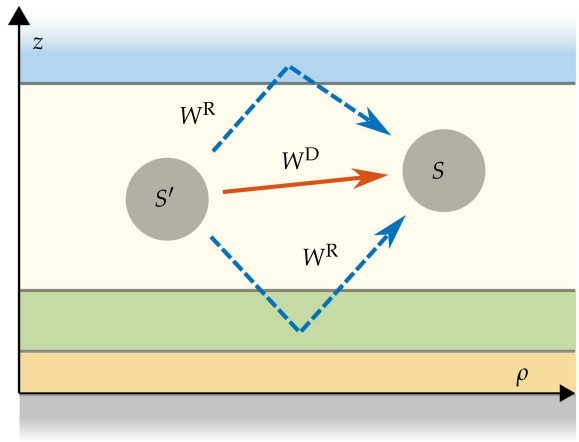

Fig. 1. Schematic view on the direct (red) and layer system mediated (dashed, blue) contributions to the coupling matrix $W^{ss'}_{nn'}$.

The present paper aims at an efficient way to evaluate the coupling matrix $W^{ss'}_{nn'}$. The latter is given by the sum

$$W^{ss'}_{nn'} = W^{\mathrm{D},ss'}_{nn'} + W^{\mathrm{R},ss'}_{nn'}$$

of a direct contribution $W^{\mathrm{D},ss'}_{nn'}$ (the coupling term for an infinite medium) and a layer system mediated term $W^{\mathrm{R},ss'}_{nn'}$, representing the wave's (multiple) reflections at the layer interfaces which are then incident at particle s, see Fig. 1.

Whereas both recursive and closed form expressions exist for the direct interaction term [11,18], each entry of $W^{\mathrm{R},ss'}_{nn'}$ involves the numerical evaluation of a Sommerfeld integral. As the number of entries is $N^2 n^2_{\max}$ and can exceed several billion for an ensemble of a few thousand wavelength scale particles, a carefully designed quadrature strategy is crucial. In the following sections, we will present an efficient way to assemble the coupling matrices by means of interpolation from a lookup table in combination with a quadrature scheme that relies on the fast Fourier algorithm and singularity extraction techniques. This way, a significant speedup can be achieved in comparison with direct contour integration in the complex plane.

3. LOOKUP TABLES

The layer system mediated coupling matrix is given by

$$W^{\mathrm{R},ss'}_{nn'} = 4\mathrm{i}^{|m'-m|}\mathrm{e}^{\mathrm{i}(m'-m)\phi_{s's}} \times (I^{+}_{nn'}(\rho_{s's}, z_s + z_{s'}) + I^{-}_{nn'}(\rho_{s's}, z_s - z_{s'})), \quad (5)$$

with $\rho_{s's}$ and $\phi_{s's}$ denoting the radial and angular cylindrical coordinates of $\mathbf{r}_s - \mathbf{r}_{s'}$ and

$$I^{\pm}_{nn'}(\rho, z) = \int_0^\infty \mathrm{d}\kappa f^{\pm}_{nn'}(\kappa, z) J_{|m'-m|}(\kappa\rho), \quad (6)$$

where

$$f^{+}_{nn'}(\kappa, z) = \frac{\kappa}{k_z k}\sum_j (B^{+\dagger}_{n,j}(L^{i_s}_j)_{12}B^{-}_{n',j}\mathrm{e}^{\mathrm{i}k_z z} + B^{-\dagger}_{n,j}(L^{i_s}_j)_{21}B^{+}_{n',j}\mathrm{e}^{-\mathrm{i}k_z z}), \quad (7)$$

$$f^{-}_{nn'}(\kappa, z) = \frac{\kappa}{k_z k}\sum_j (B^{+\dagger}_{n,j}(L^{i_s}_j)_{11}B^{+}_{n',j}\mathrm{e}^{\mathrm{i}k_z z} + B^{-\dagger}_{n,j}(L^{i_s}_j)_{22}B^{-}_{n',j}\mathrm{e}^{-\mathrm{i}k_z z}). \quad (8)$$

In the above, j denotes the plane wave polarization (TE or TM), whereas k, κ, and k_z are the wavenumber and the wave vector's radial cylindrical and z component in the scattering particle layer, respectively, $B^{\pm}_{n,j}$ are the transformation coefficients between spherical and plane vector wave functions, and $L^{i_s}_j$ is the layer system transition matrix, i.e., a generalized reflection coefficient encoding the overall response of the plane layer interfaces. A brief derivation of Eq. (5) is given in Appendix B. Apart from notation and conventions, it is analogous to the treatment presented in [13].

Note that the above integrals $I^{+}_{nn'}$ and $I^{-}_{nn'}$ only depend on two parameters: the radial relative position and the sum or the difference of the z position of the particles s and s', respectively. For scattering problems involving a large number of particles, it is therefore advantageous to precompute the integrals in a lookup table for interpolation in ρ and z, which results in a smaller number of integral evaluations. Another advantage in the use of lookup tables is that they are independent of the specific particle locations and can be reused in repeated simulations for modified particle configurations, e.g., in an ensemble averaging process for random media. Finally, as the lookup tables can be defined on a regular grid in ρ, they enable the use of the fast Fourier transform for the calculation of their entries, as will be discussed in the next section.

4. EVALUATION OF THE SOMMERFELD INTEGRALS

The Sommerfeld integrals $I^{\pm}_{nn'}$ represent Hankel transforms of order $|m' - m|$, with m being the azimuthal multipole coefficient of the respective spherical vector wave. A number of efficient techniques for the evaluation of such integrals has been published in literature; some are reviewed in [19]. In the following, we will present a dual strategy. For intermediate and large ρ, it relies on an efficient technique, which is based on the FFT in combination with singularity extraction. As this method yields accurate results only for moderate and large values of ρ, we use direct integration along a deflected contour for the computation of $I^{\pm}_{nn'}$ when ρ is small. The combination of both approaches results in a fast and accurate method to compute the complete lookup tables.

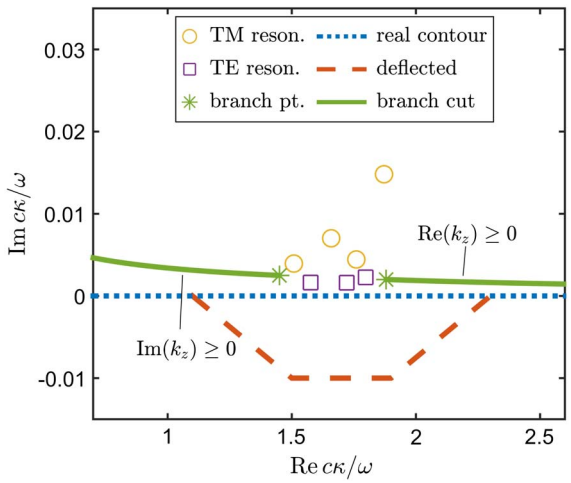

Fig. 2. Waveguide resonances and branchpoints in the complex plane. The dotted and dashed lines show the original integral contour and a deflected contour, respectively. For singularity extraction, the square-root sign is selected such that no branch cut separates the singularities from the real axis.

A. Direct Integration Along a Deflected Contour

A straightforward and robust approach is direct numerical quadrature (e.g., using the trapezoidal rule) in combination with a deflection of the integration contour into the negative complex half plane [16]. Whereas for host material refractive indices with at least a small positive imaginary part, $f^{\pm}_{nn'}$ is finite on the positive real axis, singularities are typically located in the upper complex half plane nearby the positive real axis (see Fig. 2), such that the integrand exhibits fast variations. A deflected complex integration contour that avoids the vicinity of these singularities can, therefore, lead to a better convergence of the quadrature and does not compromise the result, according to Cauchy's theorem. However, the direct integration approach still requires one numerical quadrature for each entry of the lookup table, thus causing large computational effort.

B. Asymptotic Expansion of the Bessel Function

The advantage of using the FFT to evaluate the integrals $I^{\pm}_{nn'}$ is that a large number of arguments ρ can be considered simultaneously, which results in a high computational efficiency. The strategy presented here is based on a method discussed in [19–21] (see also [16,22]). The starting point is to approximate the Bessel function according to

$$J_\nu(x) \approx \sqrt{\frac{2}{\pi x}}\cos\left(x - \frac{1}{2}\pi\nu - \frac{1}{4}\pi\right). \quad (9)$$

In principle, higher-order terms of the asymptotic expansion of J_ν could be considered, too [19]. For a function $f(x)$ defined for positive x, the domain of definition can be extended to the negative by defining [20]

$$\widehat{f}(x) = \begin{cases} f(x) & \text{for } x \geq 0 \\ f(-x)\mathrm{e}^{\mathrm{i}\pi\nu+\frac{\mathrm{i}}{2}\pi} & \text{for } x < 0. \end{cases}$$

Then, one can approximate

$$\int_0^\infty \mathrm{d}x f(x) J_\nu(xy) \approx \frac{\mathrm{e}^{-\frac{\mathrm{i}}{2}\pi\nu-\frac{\mathrm{i}}{4}\pi}}{\sqrt{2\pi y}} \int_{-\infty}^{\infty} \mathrm{d}x \frac{\widehat{f}(x)}{\sqrt{|x|}} \mathrm{e}^{\mathrm{i}xy}, \tag{10}$$

which can be evaluated by means of FFT. Note that, in general, it is not advisable to simply approximate the values of a Fourier integral by the corresponding discrete Fourier transform. Errors of the order $y\Delta x$ are expected to arise, where Δx is the sampling of $\widehat{f}(x)$ in the discrete Fourier transform. Instead, more sophisticated approaches are described in [23].

As the FFT requires an integration path along the real axis, a deflection into the complex is not permitted. In order to cancel the peaks in the integrand, we subtract a function from the integrand that has the same singular and small argument behavior as $f^{\pm}_{nn'}$ and an analytically known Hankel transform.

C. Waveguide Singularities

Guided modes in a planarly layered medium manifest themselves as pole singularities in the layer system transition matrix $L^{i_s}_j$. The weaker the damping and the larger the decay length of a specific mode, the closer is the corresponding singularity to the real axis. A pole-finding algorithm [24] based on contour integration along closed loops is employed to determine the complex locations κ_P of the poles and also the corresponding residues $\mathrm{Res}(L^{i_s}_j, \kappa_P)$. Note that, in the evaluation of the reflection and transmission coefficients at the various layer interfaces, one needs to be careful to pick the square-root sign for each layer's wave-vector z component such that no branch cut separates κ_P from the real axis, e.g., by defining for layer i with refractive index n_i:

$$k_{z,i} = \sqrt{\frac{n_i^2\omega^2}{c^2} - \kappa^2}$$

with

$$\left\{ \begin{array}{l} \mathrm{Re}\, k_{z,i} \geq 0 \\ \mathrm{Im}\, k_{z,i} \geq 0 \end{array} \right\} \quad \text{if} \quad \left\{ \begin{array}{l} \mathrm{Re}\, n_i\omega/c \geq \mathrm{Re}\, \kappa_P \\ \mathrm{Re}\, n_i\omega/c < \mathrm{Re}\, \kappa_P \end{array} \right\}.$$

This way, the pole-finding algorithm operates on the Riemann sheet, which is continuously connected to the real axis. In order to extract the singular behavior of these poles, we subtract the term

$$f_{P,\nu}(\kappa) = \frac{\kappa^{\nu+1}}{\kappa^M - \kappa_P^M},$$

for $\nu = |m - m'|$ and some even number M that fulfills $M > |m - m'| + 1$ and $M < 2\pi/\arg\kappa_P$. The above expression is a generalization of the pole-extraction functions suggested in [25,26] for the evaluation of the multilayer Green's function. $f_{P,\nu}$ has M simple poles at

$$\kappa_{P,\mu} = \kappa_P \exp\left(2\pi\mathrm{i}\frac{\mu}{M}\right), \quad \mu = 0, \ldots, M-1$$

with residue

$$\mathrm{Res}(f_{P,\nu}(\kappa), \kappa_{P,\mu}) = \kappa_{P,\mu}^{\nu+1} \prod_{\mu' \neq \mu} (\kappa_{P,\mu} - \kappa_{P,\mu'})^{-1}.$$

Following [27], the Hankel transform of $f_{P,nn'}$ is

$$\begin{aligned} F_{P,\nu}(\rho) &= \int_0^\infty \mathrm{d}\kappa f_{P,\nu}(\kappa) J_\nu(\kappa\rho) \\ &= \pi\mathrm{i} \sum_{\mu=0}^{\frac{M}{2}-1} \mathrm{Res}(f_{P,\nu}(\kappa), \kappa_{P,\mu}) H_\nu^{(1)}(\kappa_{P,\mu}). \end{aligned} \tag{11}$$

The above formula is only valid in a lossy waveguide structure, i.e., when the κ_P have a nonzero imaginary part.

D. Branchpoint Singularity

In general, the integrand of $I^{\pm}_{nn'}$ has a singularity at $\kappa = k$, i.e., at the particle layer wavenumber, where $k_z = 0$. In Eqs. (7) and (8), the singular behavior of the integrand appears explicitly in the term k_z^{-1}. In addition, the layer system transition matrix $L^{i_s}_j$ can have a pole at $k_z = 0$. The total singular behavior of $f^{\pm}_{nn'}$ around $\kappa = k$ can, thus, be written as a Laurent expansion in terms of k_z:

$$f^{\pm}_{nn'}(\kappa, z) = \frac{R^{\pm}_{\mathrm{B2},nn'}(z)}{k_z^2} + \frac{R^{\pm}_{\mathrm{B1},nn'}(z)}{k_z} + \text{regular}.$$

The coefficients $R^{\pm}_{\mathrm{B1},nn'}$ and $R^{\pm}_{\mathrm{B2},nn'}$ can be determined by means of a series expansion of all factors of $f^{\pm}_{nn'}$ around $k_z = 0$. In the evaluation of $L^{i_s}_j$, the square-root convention for $k_{z,i}$ in all other layers again needs to be chosen such that no other branch cut separates the $\kappa = k$ branch point from the real axis. Further, $L^{i_s}_j$ is typically defined recursively and can be a quite involved function of k_z. Computer programs that allow symbolic manipulations facilitate the automatic evaluation of the series expansions.

The singularity proportional to $R^{\pm}_{\mathrm{B2},nn'}$ is a simple pole at $\kappa = k$, as $k_z^2 = (k - \kappa)(k + \kappa)$. Thus, it can be extracted by the same function as the waveguide poles:

$$f_{\mathrm{B2},\nu}(\kappa) = \frac{\kappa^{\nu+1}}{\kappa^M - k^M}.$$

The Hankel transform $F_{\mathrm{B2},\nu}(\rho)$ of this function can be found in analogy to Eq. (11). For the compensation of the algebraic singularity proportional to $R^{\pm}_{\mathrm{B1},nn'}$, we suggest to use

$$f_{\mathrm{B1}}(\kappa) = \frac{1}{k_z} + \frac{\mathrm{i}}{\sqrt{\kappa^2 + k^2}}.$$

The first term is to cancel the singularity, and the second term ensures that f_{B1} decays sufficiently fast for $\kappa \to \infty$. In order to evaluate the Hankel transform, both terms can be rewritten in the form $(\kappa^2 + a^2)^{-1/2}$, the transform of which can be found in [28], to give

$$\begin{aligned} F_{\mathrm{B1},\nu}(\rho) &= \int_0^\infty \mathrm{d}\kappa f_{\mathrm{B1}}(\kappa) J_\nu(\kappa\rho) \\ &= -\mathrm{i} I_{\nu/2}\left(\frac{-\mathrm{i}k\rho}{2}\right) K_{\nu/2}\left(\frac{-\mathrm{i}k\rho}{2}\right) \\ &\quad + \mathrm{i} I_{\nu/2}\left(\frac{k\rho}{2}\right) K_{\nu/2}\left(\frac{k\rho}{2}\right). \end{aligned}$$

Here, I_n and K_n denote the modified Bessel functions of the first and second kind, respectively.

E. Singularity Extraction

Extracting all singularities that are located nearby the positive real axis from the function $f^{\pm}_{nn'}$ yields

$$\tilde{f}^{\pm}_{nn'}(\kappa,z) = f^{\pm}_{nn'}(\kappa,z) - \sum_P C^{\pm}_{P,nn'}(z) f_{P,|m-m'|}(\kappa) - C^{\pm}_{\mathrm{B1},nn'}(z) f_{\mathrm{B1}}(\kappa) - C^{\pm}_{\mathrm{B2},nn'}(z) f_{\mathrm{B2}}(\kappa),$$

where the extraction functions have been multiplied by appropriate coefficients C to cancel the respective singular behavior of $f^{\pm}_{nn'}$,

$$C^{\pm}_{P,nn'}(z) = \frac{\mathrm{Res}(f^{\pm}_{nn'}(\kappa,z),\kappa_P)}{\mathrm{Res}(f_{P,|m-m'|}(\kappa),\kappa_P)}$$
$$C^{\pm}_{\mathrm{B1},nn'}(z) = R^{\pm}_{\mathrm{B1},nn'}(z)$$
$$C^{\pm}_{\mathrm{B2},nn'}(z) = -\frac{R^{\pm}_{\mathrm{B2},nn'}(z)}{2k\,\mathrm{Res}(f_{\mathrm{B2},|m-m'|}(\kappa),k)}.$$

The so-defined singularity extracted function $\tilde{f}^{\pm}_{nn'}$ is finite at all resonance locations $\kappa = \kappa_P$ as well as at $\kappa = k$. It can, in principle, be inserted into the Hankel transform prescription according to Eq. (10). However, as the asymptotic expansion Eq. (9) of the Bessel function is valid only for large arguments, the accuracy of Eq. (10) will be higher if the integrand function is small around $x = 0$. To achieve this, we subtract another function in order to cancel the small argument behavior.

F. Small Argument Suppression

Consider, e.g.,

$$f_{\mathrm{E1}}(\kappa) = \exp(-a_1\kappa),$$
$$f_{\mathrm{E2}}(\kappa) = \exp(-a_2\kappa^2).$$

For suitable positive numbers $a_{1,2}$, these functions decay sufficiently fast and can be used to cancel the constant and linear term of the Taylor series for $\tilde{f}^{\pm}_{nn'}$ around $\kappa = 0$. The Hankel transform of these correction functions can be found in [28]:

$$F_{\mathrm{E1},\nu}(\rho) = \int_0^\infty \mathrm{d}\kappa f_{\mathrm{E1}}(\kappa) J_\nu(\kappa\rho) = \frac{\left(\sqrt{a_1^2+\rho^2} - a_1\right)^\nu}{\rho^\nu \sqrt{a_1^2+\rho^2}}$$
$$F_{\mathrm{E2},\nu}(\rho) = \int_0^\infty \mathrm{d}\kappa f_{\mathrm{E2}}(\kappa) J_\nu(\kappa\rho) = \sqrt{\frac{\pi}{4a_2}} \exp\left(-\frac{\rho^2}{8a_2}\right) I_{\nu/2}\left(\frac{\rho^2}{8a_2}\right).$$

The small argument suppression yields the regularized function:

$$f^{\pm}_{\mathrm{reg},nn'}(\kappa,z) = \tilde{f}^{\pm}_{nn'}(\kappa,z) - C^{\pm}_{\mathrm{E1},nn'}(z) f_{\mathrm{E1}}(\kappa) - C^{\pm}_{\mathrm{E2},nn'}(z) f_{\mathrm{E2}}(\kappa),$$

where the coefficients C are chosen such that the function value and the first derivative of $\tilde{f}^{\pm}_{nn'}$ are exactly cancelled at $\kappa = 0$:

$$C^{\pm}_{\mathrm{E1},nn'}(z) = -\frac{1}{a_1}\frac{\partial \tilde{f}^{\pm}_{nn'}(0,z)}{\partial\kappa}$$
$$C^{\pm}_{\mathrm{E2},nn'}(z) = \frac{1}{2a_2}\left(a_1^2 C^{\pm}_{\mathrm{E1},nn'}(z) - \frac{\partial^2 \tilde{f}^{\pm}_{nn'}(0,z)}{\partial\kappa^2}\right).$$

In principle, more terms of the Taylor expansion could be cancelled in order to further increase the accuracy of the method.

Finally, the regularized function $f^{\pm}_{\mathrm{reg},nn'}$ is well suited for numerical Hankel transformation according to Eq. (10). Thus, the Sommerfeld integrals Eq. (6) can be evaluated as

$$I^{\pm}_{nn'}(\rho,z) \approx \frac{\mathrm{e}^{-\frac{1}{2}\pi|m-m'|-\frac{1}{4}\pi}}{\sqrt{2\pi\rho}} \int_{-\infty}^{\infty} \mathrm{d}\kappa \frac{\widehat{f}^{\pm}_{\mathrm{reg},nn'}(\kappa,z)}{\sqrt{|\kappa|}} \mathrm{e}^{\mathrm{i}\kappa\rho} + I^{\pm}_{C,nn'}(\rho,z), \tag{12}$$

where the integral expression is evaluated by means of FFT, and the correction term $I^{\pm}_{C,nn'}$ is given by

$$I^{\pm}_{C,nn'}(\rho,z) = \sum_P C^{\pm}_{P,nn'}(z) F_{P,|m-m'|}(\rho) + C^{\pm}_{\mathrm{B1},nn'}(z) F_{\mathrm{B1},|m-m'|}(\rho) + C^{\pm}_{\mathrm{B2},nn'}(z) F_{\mathrm{B2},|m-m'|}(\rho) + C^{\pm}_{\mathrm{exp},nn'}(z) F_{\mathrm{exp},|m-m'|}(\rho) + C^{\pm}_{G,nn'}(z) F_{G,|m-m'|}(\rho).$$

The procedure of singularity extraction and small argument suppression comes at the price of a slower decay of $f^{\pm}_{\mathrm{reg}}(\kappa)$ for large κ (see Fig. 3). However, this is not critical because, for a fine resolution of the lookup tables in ρ, a large truncation scale of the FFT integral in Eq. (12) is required anyway.

5. EXEMPLARY RESULTS

The above scheme was implemented into a MATLAB routine and applied to a test scenario representing a typical OLED geometry with a scattering particle layer for outcoupling. The layer system (see Fig. 4) consists of a glass substrate ($n_{\mathrm{g}} = 1.5$), a 500 nm thick host layer ($n_{\mathrm{h}} = 1.8 + 10^{-4}\mathrm{i}$) for the scattering particles, a 150 nm transparent electrode ($n_{\mathrm{t}} = 1.9 + 0.005\mathrm{i}$), a 100 nm active (organic) layer ($n_{\mathrm{a}} = 1.75$), and a metallic back electrode ($n_{\mathrm{m}} = 1 + 6\mathrm{i}$). N spherical scattering particles with radius $R_s = 100$ nm and refractive index $n_s = 2.5$ are located inside the host layer; the particle positions are chosen randomly within a cylindrical volume employing a non-overlap condition with the other particles and the layer interfaces. The lateral dimension of the particle cluster is adapted to yield a volume density of 4% in the scattering layer. A horizontally oriented electric point dipole located in the middle of the emitter layer and emitting at a vacuum wavelength of $\lambda_0 = 520$ nm (which corresponds to a vacuum wavenumber $k_0 = \omega/c = 2\pi/\lambda_0$) serves as the initial excitation source. The dimensionless size parameter of the particles in the host medium is, thus, $R_s n_{\mathrm{h}} k_0 \approx 2.2$. For homogeneous spherical scattering particles, the T-matrix is diagonal and contains the Mie coefficients, which can be evaluated analytically [11]. All calculations are performed on a Linux-run workstation, equipped with an Intel i7-3930K processor, 64 GB RAM, and an NVIDIA GeForce GTX 970 GPU, which is used for the FFT computations. In the following, we will present the results and comment on the achieved accuracy and the required computing time.

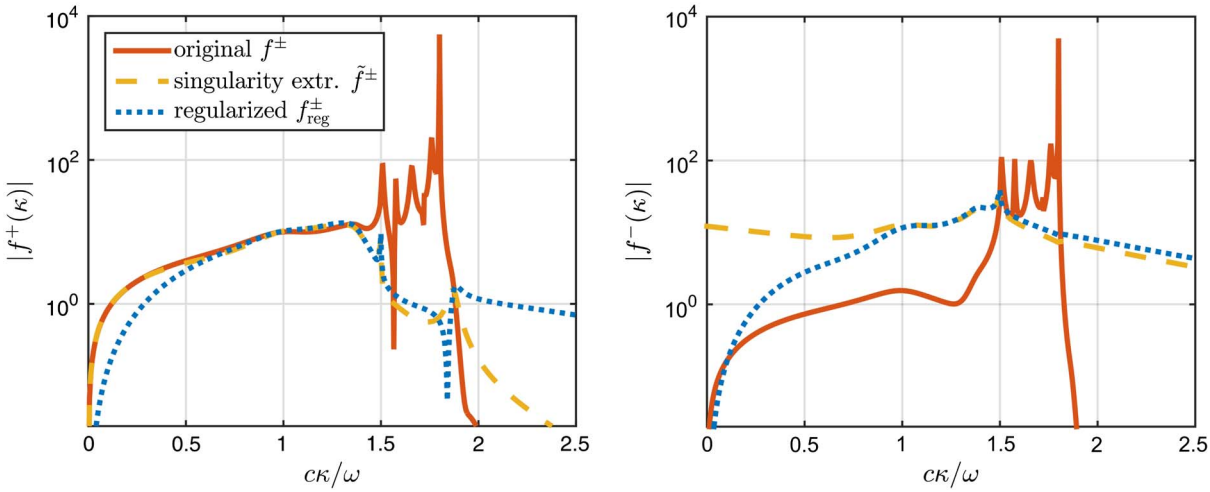

Fig. 3. Functions $f^{+}(\kappa)$ (left) and $f^{-}(\kappa)$ (right) before and after singularity extraction and small argument suppression.

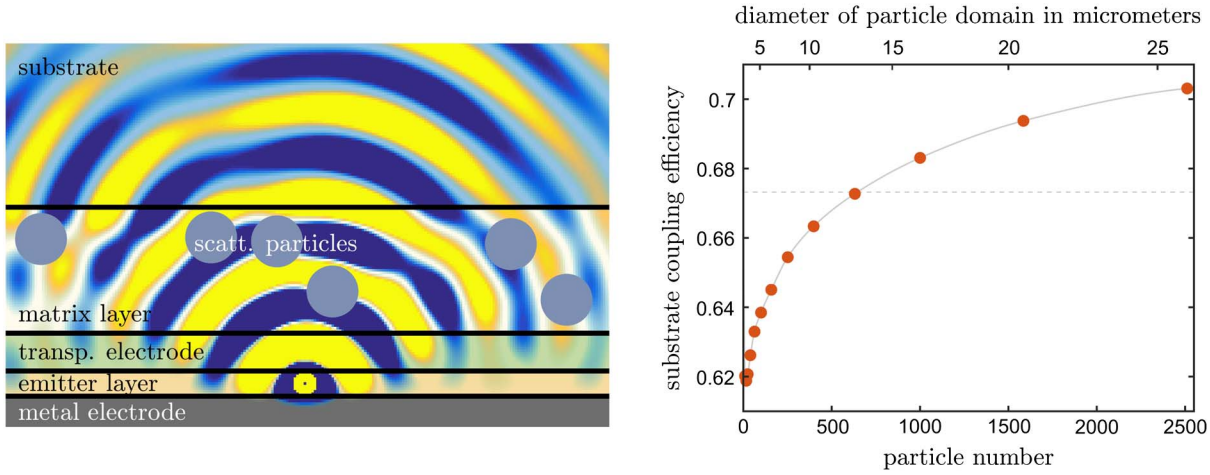

Fig. 4. Left: OLED geometry and exemplary field distribution. Right: simulated substrate coupling efficiency as a function of the particle number. The dashed line indicates the substrate coupling efficiency in the absence of scattering particles. Due to shadowing, particles close to the dipole have a negative effect on the substrate coupling efficiency. For larger samples, this is more than compensated for by outcoupling effects from the waveguide modes. The particles then have a positive net effect.

A. Assembly of the $I^{\pm}_{nn'}$ Lookup Table

The lookup tables for the Sommerfeld integrals require the computation of $I^{\pm}_{nn'}(\rho, z)$ on a grid (ρ_i, z_i), where ρ runs from 0 to some maximal distance $\rho_{\max}$, and the z_i cover all possible values for $z_s \pm z_{s'}$. The resolution in both ρ and z should be sufficiently fine to allow an accurate interpolation. We choose $\Delta\rho \approx \Delta z \approx \lambda_0/50$. For the FFT, the integrand $f^{\pm}_{\mathrm{reg}}(\kappa, z)$ is evaluated along the real axis between $\kappa = 0$ and $\kappa_{\max} = 25k_0$ in steps of $\Delta\kappa = 10^{-4}k_0$. It is necessary to sample the integrand with a rather fine resolution because despite the singularity extraction, $f^{\pm}_{\mathrm{reg}}$ exhibits some sharp features, e.g., around the branch points. One side effect of the very fine sampling of the integrand is that we can safely approximate the Fourier integral directly by the discrete Fourier transform, as the associated numerical error mentioned in Section 4B only affects values of $I^{\pm}_{nn'}$ for radial distances ρ large compared with the maximal particle separation. However, note that, if the method described here is applied to very large radial particle distances, the Fourier integral 10 should be evaluated according to [23].

Further, a large enough truncation scale is required for a fine resolution in ρ, as $\Delta\rho \sim \pi/\kappa_{\max}$. In fact, the quadrature strategy based on FFT requires considerably more integrand evaluations than would be necessary for direct integration along a deflected contour. However, this disadvantage is more than compensated by the fact that by means of FFT, many thousand Sommerfeld integral evaluations can be simultaneously performed. As the asymptotic approximation of the Bessel function, Eq. (9) is not valid for small arguments, the evaluation of the Sommerfeld integrals by means of the method described in Section B is not accurate for small lateral separation ρ. Therefore, it is necessary to accomplish this approach with a more robust quadrature technique. For this purpose, direct integration by means of the trapezoidal rule is used in combination with a slight deflection of the integral contour near the

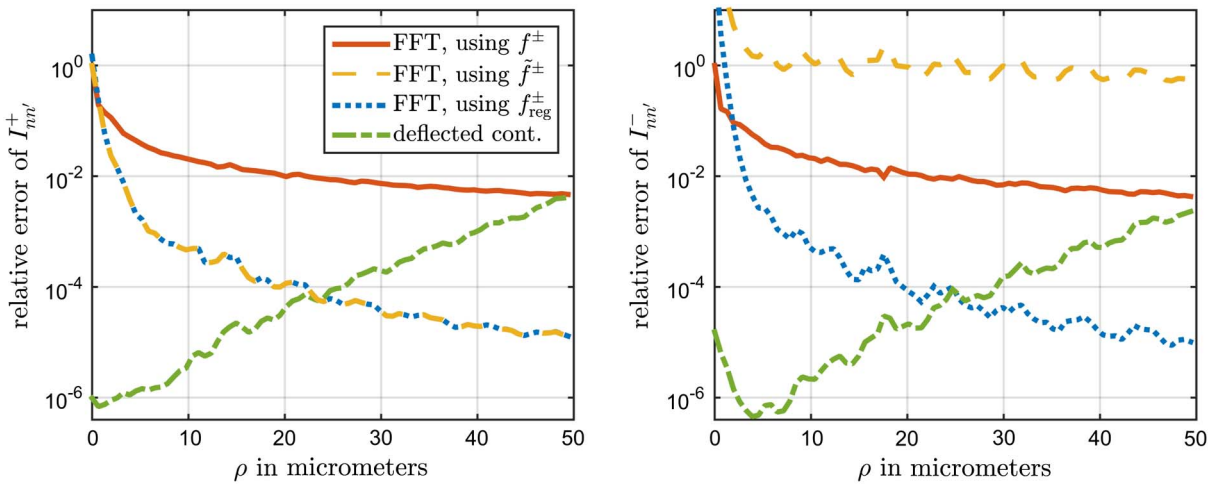

Fig. 5. Relative error of the Sommerfeld integrals using an asymptotic approximation of the Bessel function in combination with FFT without (red) and with (dashed, yellow) singularity extraction and after small argument suppression (dotted, blue). The dashed–dotted green line refers to the trapezoidal rule along a deflected contour with a sampling of $\Delta\kappa = 10^{-3}k_0$.

singularities into the lower half-plane. The sampling rate is set to $\Delta\kappa = 10^{-3}k_0$, and the integrals are truncated at $\kappa_{\max} = 3k_0$.

Figure 5 shows the accuracy of the Sommerfeld integrals evaluated by means of FFT with and without singularity extraction as well as from direct integration along a deflected contour. The depicted relative errors have been estimated by comparison to baseline results from direct contour integration with a fine sampling of the integrand, $\Delta\kappa = 5 \times 10^{-4}k_0$, and a large truncation scale, $\kappa_{\max} = 6k_0$. As a measure for the deviation between the resulting matrices, we used the Euclidean norm. It turns out that, in the case of $I^{+}_{nn'}$, the small argument suppression makes no difference, whereas it proves to be essential in the case of $I^{-}_{nn'}$. Aiming at an accuracy of, e.g., 0.5%, the results from the asymptotic approximation of the Bessel functions in combination with singularity extraction and small argument suppression can be used starting from a minimal separation, $\rho_0 \approx 10\lambda_0$, for the given example. For smaller values of ρ, direct integration along a deflected contour is applied. Fortunately, in this regime the direct integration along a deflected contour is robust even for a relatively sparse sampling of the integrand, as the oscillations resulting from the Bessel function $J_\nu(\kappa\rho)$ are rather slow.

B. Accuracy and Effort

In order to assess the simulation accuracy, we evaluate the substrate coupling efficiency, i.e., the power radiated into the substrate far field divided by the total dissipated power (see Fig. 4). This quantity is an important figure of merit for the OLED design, as it reflects the incomplete extraction of generated photons due to absorption and losses into waveguide modes. This way, the simulation result is represented by a single quantity, the relative deviation of which can be used as an accuracy benchmark. In the test simulations, the maximal polar multipole order is set to $l_{\max} = 3$, which corresponds to $n_{\max} = 30$. Furthermore, we perform reference simulations with $l_{\max} = 4$ ($n_{\max} = 48$), which serve as a baseline for the accuracy estimation. For the reference simulation, we calculate W^{R} using direct integration along a deflected contour (i.e., without the use of a lookup table) with a sampling of $\Delta\kappa = 5 \times 10^{-4}k_0$ and a truncation at $\kappa_{\max} = 6k_0$. It turns out that the estimated relative error of the results from method presented here is below 10^{-4} and in the same range as for direct calculation of W^{R} for $l_{\max} = 3$.

Regarding computational efficiency, Fig. 6 depicts the simulation time for the dual strategy presented here in comparison with the direct calculation of W^{R}.

Note that the runtime results displayed in Fig. 6 depend on the specific geometry as well as on the choice of the numerical parameters that determine the accuracy of the respective calculations. For a fixed volume density, the radius of the cylindrical domain filled with particles scales like $N^{1/2}$, whereas the effort

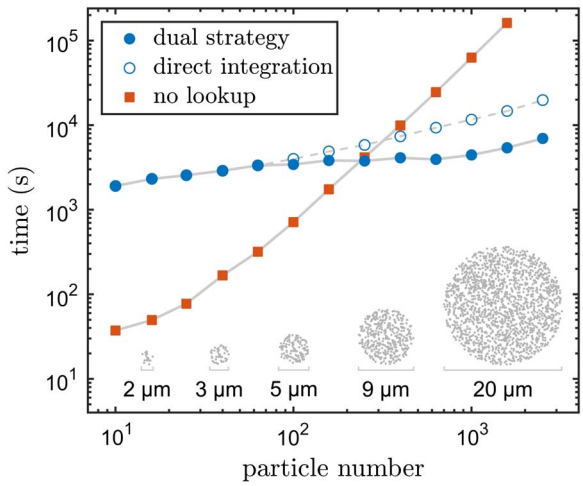

Fig. 6. Simulation runtime for the computation of the substrate coupling efficiency in an OLED geometry with N scattering particles. The dual strategy presented here of Sommerfeld integration in combination with a lookup-table approach (filled circles) is compared with direct calculation of the coupling coefficients (squares). The empty circles correspond to a lookup assembly by direct integration along a deflected contour only, i.e., without the use of the FFT results. The insets illustrate the particle distribution's lateral dimension in the scattering layer.

for a direct calculation of W^{R} scales such as N^2. Thus, a lookup table is, in general, most efficient for large N, whereas for small N, direct calculation of W is to be preferred. As soon as the lateral dimension of the particle distribution exceeds ρ_0, the lookup table can in part be filled by the FFT results, yielding significantly faster simulations compared to the direct integration approach. Then, the time needed to generate the lookup table is independent of the number of particles for a wide range of N. An increased number of scattering particles only affects the time required for the interpolation as well as the time used for the solution of the linear system as well as the post-processing.

6. CONCLUSIONS

A strategy for the efficient evaluation of Sommerfeld integrals for the simulation of electromagnetic scattering at large ensembles of wavelength-scale particles within a planarly layered medium was presented. Asymptotic approximation in combination with FFT and a table-lookup approach have resulted in a significant speed-up of the calculations. We have demonstrated that singularity extraction and small argument suppression are crucial for the accuracy of the presented method. As an exemplary application, we have simulated light outcoupling from an OLED. The substrate coupling efficiency of an OLED geometry with 2500 wavelength-scale particles was modeled with a relative precision better than 10^{-4} within 2 h runtime on a workstation computer. The lookup-table approach also allows for cost-efficient averaging over several random particle configurations, such that efficient optimization and rigorous studies of the statistical properties of large random particle layers in a thin film system become feasible.

APPENDIX A: VECTOR WAVE FUNCTIONS

The plane vector wave functions (PVWFs) are defined as

$$\mathbf{E}_1(\mathbf{k};\mathbf{r}) = \exp(\mathrm{i}\mathbf{k}\cdot\mathbf{r})\widehat{\mathbf{e}}_\alpha,$$
$$\mathbf{E}_2(\mathbf{k};\mathbf{r}) = \exp(\mathrm{i}\mathbf{k}\cdot\mathbf{r})\widehat{\mathbf{e}}_\beta,$$

where $\widehat{\mathbf{e}}_\alpha$ and $\widehat{\mathbf{e}}_\beta$ denote the angular unit vectors in azimuthal and polar direction, respectively. Further, the spherical vector wave functions (SVWFs) are defined as [11]

$$\mathbf{M}^{(\nu)}_{lm1}(\mathbf{r}) = \frac{1}{\sqrt{2l(l+1)}}\nabla\times(\mathbf{r}z^{(\nu)}_l(kr)P^{|m|}_l(\cos\theta)\mathrm{e}^{\mathrm{i}m\phi}),$$
$$\mathbf{M}^{(\nu)}_{lm2}(\mathbf{r}) = \frac{1}{k}\nabla\times\mathbf{M}^{(\nu)}_{ml1}(\mathbf{r}).$$

Here, the radial wave function $z^{(\nu)}_l$ stands either for the spherical Bessel function of order l, $z^{(1)}_l = j_l$ (regular SVWF), or the spherical Hankel function of first kind, $z^{(3)}_l = h^{(1)}_l$ (outgoing SVWF). As before, $k = nk_0$ is the wavenumber and P^m_l denote the normalized associated Legendre functions, and (r,θ,ϕ) are the spherical coordinates of the position vector $\mathbf{r}$. The outgoing SVWF can be transformed into PVWFs using [11]

$$\mathbf{M}^{(3)}_{mlp}(\mathbf{r}) = \frac{1}{2\pi}\int \mathrm{d}^2\mathbf{k}_\parallel \frac{1}{k_z k}\sum_{j=1}^{2} B^m_{lpj}(\pm k_z/k)\mathbf{E}_j(\mathbf{k}^\pm;\mathbf{r})\mathrm{e}^{\mathrm{i}m\alpha} \quad \text{for } z\gtrless 0, \tag{A1}$$

with

$$B^m_{lpj}(x) = \frac{1}{\mathrm{i}^{l+1}}\frac{1}{\sqrt{2l(l+1)}}(\mathrm{i}\delta_{j1}+\delta_{j2}) \times\left(\delta_{pj}\sqrt{1-x^2}\frac{\partial P^{|m|}_l(x)}{\partial x} + (\delta_{pj}-1)m\frac{P^{|m|}_l(x)}{\sqrt{1-x^2}}\right). \tag{A2}$$

In the above, $\mathbf{k}^\pm$ stands for the wave vector in the case of up- and downward propagation, respectively, i.e., $\mathbf{k}^\pm\cdot\widehat{\mathbf{e}}_z = \pm k_z$ with $k_z = \sqrt{k^2-\kappa^2}$. The integral is understood to run over the in-plane components of the wave vector, i.e., $\int \mathrm{d}^2\mathbf{k}_\parallel = \int_{-\infty}^{\infty}\mathrm{d}k_x\int_{-\infty}^{\infty}\mathrm{d}k_x$. On the other hand, the expansion of a PVWF in terms of regular SVWF reads:

$$\mathbf{E}^\pm_j(\kappa,\alpha;\mathbf{r}) = 4\sum_{l=1}^{\infty}\sum_{m=-l}^{l}\mathrm{e}^{-\mathrm{i}m\alpha}\sum_{p=1}^{2}B^{m\dagger}_{lpj}(\pm k_z/k)\mathbf{M}^{(1)}_{mlp}(\mathbf{r}). \tag{A3}$$

The matrix $B^\dagger$ has all the explicit i in Eq. (A2) set to –i.

APPENDIX B: LAYER SYSTEM MEDIATED PARTICLE COUPLING

In general, the (outgoing) field of a localized excitation can be written in the form

$$\mathbf{E}_{\mathrm{exc}}(\mathbf{r}) = \sum_j\int \mathrm{d}^2\mathbf{k}_\parallel g^\pm_{\mathrm{exc},j}(\mathbf{k}_\parallel)\mathbf{E}_j(\mathbf{k}^\pm;\mathbf{r}) \quad \text{for } z\gtrless z_{\mathrm{exc}}, \tag{B1}$$

where z_{exc} denotes the z position of the excitation. Then, the electric layer system response, evaluated in the exciting layer i_{exc}, can be conveniently cast into a two-vector scheme:

$$\mathbf{E}^{\mathrm{R}}_{\mathrm{exc}}(\mathbf{r}) = \sum_j\int \mathrm{d}^2\mathbf{k}_\parallel[\mathbf{E}_j(\mathbf{k}^+;\mathbf{r}),\mathbf{E}_j(\mathbf{k}^-;\mathbf{r})]\begin{bmatrix} g^{\mathrm{R},+}_{\mathrm{exc},j}(\mathbf{k}_\parallel)\\ g^{\mathrm{R},-}_{\mathrm{exc},j}(\mathbf{k}_\parallel)\end{bmatrix},$$

with

$$\begin{bmatrix} g^{R,+}_{\mathrm{exc},j}(\mathbf{k}_\parallel)\\ g^{R,-}_{\mathrm{exc},j}(\mathbf{k}_\parallel)\end{bmatrix} = L^{i_{\mathrm{exc}}}_j(\kappa)\begin{bmatrix} g^{+}_{\mathrm{exc},j}(\mathbf{k}_\parallel)\\ g^{-}_{\mathrm{exc},j}(\mathbf{k}_\parallel)\end{bmatrix}.$$

Here, $L^i_j(\kappa)$ denotes the 2×2 layer system transition matrix, which can be constructed by means of the transfer matrix or the scattering matrix formalism [13].

Comparing Eqs. (A1)–(B1), we find that the layer system response to an outgoing spherical wave $\mathbf{M}^{(3)}_{n'}(\mathbf{r}-\mathbf{r}_{s'})$ reads

$$\mathbf{E}^{\mathrm{R}}_{s'}(\mathbf{r}) = \sum_j\int \mathrm{d}^2\mathbf{k}_\parallel[\mathbf{E}_j(\mathbf{k}^+;\mathbf{r}),\mathbf{E}_j(\mathbf{k}^-;\mathbf{r})]\begin{bmatrix} g^{\mathrm{R},+}_{s',j}(\mathbf{k}_\parallel)\\ g^{\mathrm{R},-}_{s',j}(\mathbf{k}_\parallel)\end{bmatrix}, \tag{B2}$$

with

$$\begin{bmatrix} g^{\mathrm{R},+}_{s',j}(\mathbf{k}_\parallel)\\ g^{\mathrm{R},-}_{s',j}(\mathbf{k}_\parallel)\end{bmatrix} = \frac{\mathrm{e}^{\mathrm{i}m'\alpha}}{2\pi}\frac{1}{k_z k}\sum_{j=1}^{2}L^{i_{s'}}_j(\kappa)\begin{bmatrix} B^{m'}_{l'p'j}(k_z/k)\mathrm{e}^{-\mathrm{i}\mathbf{k}^+\cdot\mathbf{r}_{s'}}\\ B^{m'}_{l'p'j}(-k_z/k)\mathrm{e}^{-\mathrm{i}\mathbf{k}^-\cdot\mathbf{r}_{s'}}\end{bmatrix}.$$

By definition of $W^{\mathrm{R},ss'}_{nn'}$,

$$\mathbf{E}^{\mathrm{R}}_{s'}(\mathbf{r}) = \sum_n W^{\mathrm{R},ss'}_{nn'}\mathbf{M}^{(1)}_n(\mathbf{r}-\mathbf{r}_s), \tag{B3}$$

where n and n' abbreviate the multi indices (l, m, p) and (l', m', p'), respectively. Inserting Eq. (A3) into Eq. (B2) and comparing the expression with Eq. (B3) yields

$$W^{\mathrm{R},ss'}_{n,n'} = \frac{2}{\pi}\sum_j \int \frac{\mathrm{d}^2\mathbf{k}_\parallel}{k_z k}\, \mathrm{e}^{\mathrm{i}(m'-m)\alpha}\mathrm{e}^{\mathrm{i}\mathbf{k}_\parallel\cdot(\mathbf{r}_s-\mathbf{r}_{s'})} \times [B^{+\dagger}_{n,j}\mathrm{e}^{\mathrm{i}k_z z_s}, B^{-\dagger}_{n,j}\mathrm{e}^{-\mathrm{i}k_z z_s}] L^{i_s}_j \begin{bmatrix} B^{+}_{n'j}\mathrm{e}^{-\mathrm{i}k_z z_{s'}} \\ B^{-}_{n'j}\mathrm{e}^{\mathrm{i}k_z z_{s'}} \end{bmatrix}. \quad \textbf{(B4)}$$

Here, the symbols $B^{\pm}_{n,j}$ abbreviate $B^m_{lp,j}(\pm k_z/k)$. In order to carry out the α integral, we make use of $\mathrm{d}^2\mathbf{k}_\parallel = \kappa \mathrm{d}\kappa \mathrm{d}\alpha$ and $\mathbf{k}_\parallel \cdot (\mathbf{r}_s - \mathbf{r}_{s'}) = \kappa\rho_{s's}\cos(\alpha - \phi_{s's})$ where $(\rho_{s's}, \phi_{s's})$ are the polar coordinates of $\mathbf{r}_s - \mathbf{r}_{s'}$, as well as the identity [29],

$$\int_0^{2\pi} \mathrm{d}\alpha \mathrm{e}^{\mathrm{i}\nu\alpha}\mathrm{e}^{\mathrm{i}x\cos(\alpha-\phi)} = 2\pi \mathrm{i}^{|\nu|} J_{|\nu|}(x)\mathrm{e}^{\mathrm{i}\nu\phi}, \quad \textbf{(B5)}$$

to finally find Eq. (5).

Funding. Deutsche Forschungsgemeinschaft (DFG) (SPP 1839 "Tailored Disorder").

Acknowledgment. The authors wish to thank Carola Moosmann, Daniel Mackowski, and Thomas Wriedt for advice and helpful discussions, Ruben Hünig for support regarding the GPU-accelerated calculations, and the anonymous reviewer for pointing out the pitfall associated with a direct approximation of Fourier integrals by the discrete Fourier transform. A. E. acknowledges support from the Karlsruhe School of Optics & Photonics (KSOP).

REFERENCES

1. H. Bechtel, W. Busselt, and J. Opitz, "Subwavelength particle layers for improved light outcoupling of OLEDs," Proc. SPIE **5519**, 194–205 (2004).
2. H.-W. Chang, J. Lee, S. Hofmann, Y. Hyun Kim, L. Müller-Meskamp, B. Lüssem, C.-C. Wu, K. Leo, and M. C. Gather, "Nano-particle based scattering layers for optical efficiency enhancement of organic light-emitting diodes and organic solar cells," J. Appl. Phys. **113**, 204502 (2013).
3. N. Nakamura, B. Domercq, S. Billet, P. Roquiny, N. Wada, N. Fukumoto, M. Tanida, Y. Aoki, and M. Ohgawara, "Advanced glass substrate for the enhancement of OLED lighting out-coupling efficiency," SID Symp. Digest Tech. Papers **44**, 803–806 (2013).
4. J. Lee, Y. Y. Kwon, E.-H. Choi, J. Park, H. Yoon, and H. Kim, "Enhancement of light-extraction efficiency of organic light-emitting diodes using silica nanoparticles embedded in TiO_2 matrices," Opt. Express **22**, A705–A714 (2014).
5. P. C. Waterman, "Matrix formulation of electromagnetic scattering," Proc. IEEE **53**, 805–812 (1965).
6. M. I. Mishchenko, G. Videen, V. A. Babenko, N. G. Khlebtsov, and T. Wriedt, "T-matrix theory of electromagnetic scattering by partciles and its applications: a comprehensive reference database," J. Quantum Spectrosc. Radiat. Transfer **88**, 357–406 (2004).
7. D. Ko and J. Sambles, "Scattering matrix method for propagation of radiation in stratified media: attenuated total reflection studies of liquid crystals," J. Opt. Soc. Am. A **5**, 1863–1866 (1988).
8. G. Kristensson, "Electromagnetic scattering from buried inhomogeneities—a general three-dimensional formalism," J. Appl. Phys. **51**, 3486–3500 (1980).
9. J. Bobbert and P. A. Vlieger, "Light scattering by a sphere on a substrate," Physica A **137**, 209–242 (1986).
10. A. Bostrom, G. Kristensson, and S. Strom, "Transformation properties of plane, spherical and cylindrical scalar and vector wave functions," in *Field Representations and Introduction to Scattering* (Elsevier, 1991), pp. 165–210.
11. Y. A. Doicu, A. Wriedt, and T. Eremin, *Light Scattering by Systems of Particles*, 1st ed. (Springer, 2006).
12. D. W. Mackowski, "Exact solution for the scattering and absorption properties of sphere clusters on a plane surface," J. Quantum Spectrosc. Radiat. Transfer **109**, 770–788 (2008).
13. A. Egel and U. Lemmer, "Dipole emission in stratified media with multiple spherical scatterers: Enhanced outcoupling from OLEDs," J. Quantum Spectrosc. Radiat. Transfer **148**, 165–176 (2014).
14. A. Sommerfeld, "Über die Ausbreitung der Wellen in der drahtlosen Telegraphie," Ann. Phys. **333**, 665–736 (1909).
15. E. Kuester and D. Chang, "Evaluation of Sommerfeld integrals associated with dipole sources above Earth," Tech. Rep., Electromagnetics Laboratory (University of Colorado, 1979).
16. W. C. Chew, *Waves and Fields in Inhomogeneous Media* (IEEE, 1996).
17. D. W. Mackowski, "Extension of the MSTM code to particles near a surface," in *Scattering by Aggregates on Surfaces*, T. Wriedt and Y. Eremin, eds. (epubli, 2014), p. 6.
18. M. I. Mishchenko, L. D. Travis, and A. A. Lacis, *Scattering, Absorption, and Emission of Light by Small Particles* (Cambridge University, 2002).
19. M. Cree and P. Bones, "Algorithms to numerically evaluate the Hankel transform," Comput. Math. Appl. **26**, 1–12 (1993).
20. S. Candel, "Dual algorithms for fast calculation of the Fourier-Bessel transform," IEEE Trans. Acoust. Speech Signal Process. **29**, 963–972 (1981).
21. A. V. Oppenheim, "Computation of the Hankel transform using projections," J. Acoust. Soc. Am. **68**, 523–529 (1980).
22. S. Franke and G. Swenson, "A brief tutorial on the fast field program (FFP) as applied to sound propagation in the air," Appl. Acoust. **27**, 203–215 (1989).
23. W. Press, S. Teukolsky, W. Vetterling, and B. P. Flannery, *Numerical Recipes: The Art of Scientific Computing*, 3rd ed. (Cambridge University, 2007).
24. B. Hu and W. C. Chew, "Fast inhomogeneous plane wave algorithm for electromagnetic solutions in layered medium structures: Two-dimensional case," Radio Sci. **35**, 31–43 (2000).
25. F. Demuynck, G. Vandenbosch, and A. Van de Capelle, "The expansion wave concept. I. Efficient calculation of spatial Green's functions in a stratified dielectric medium," IEEE Trans. Anten. Propag. **46**, 397–406 (1998).
26. I. D. Koufogiannis, M. Mattes, and J. R. Mosig, "On the development and evaluation of spatial-domain green's functions for multilayered structures with conductive sheets," IEEE Trans. Microwave Theory Tech. **63**, 20–29 (2015).
27. Q.-G. Lin, "Infinite integrals involving Bessel functions by contour integration," Integral Trans. Spec. Funct. **24**, 783–795 (2013).
28. I. S. Gradshteyn and I. M. Ryzhik, *Table of Integrals, Series, and Products*, 7th ed. (Elsevier/Academic, 2007).
29. J. A. Stratton, *Electromagnetic Theory* (McGraw-Hill, 1941).